A Vector Sensor Receiver for Chirp Modulation in Underwater Acoustic Particle Velocity Channels

C. Chen and A. Abdi

Center for Wireless Communication and Signal Processing Research
Dept. of Electrical and Computer Engineering, New Jersey Institute of Technology, Newark, NJ 07102, USA

Email: ali.abdi@njit.edu

***Abstract* --- A chirp signal has a time varying frequency which provides better range resolution than a single frequency signal. On the other hand, vector sensors have been recently proposed for underwater acoustic communication systems as compact and efficient multichannel receivers. In this paper, linear chirp modulation is integrated with an underwater acoustic vector sensor receiver. A parametric noise model is developed for the vector sensor receiver and used to study the vector matched filter performance. The results indicate that compared to scalar receivers, a small size vector sensor receiver can significantly enhance the output of a filter matched to a linear chirp signal. This is particularly important for synchronization and signal acquisition in low SNR scenarios.**

Index Terms*— *Chirp modulation, noise modeling, underwater communication, vector sensors

I. INTRODUCTION

A chirp is a signal whose frequency varies with time. There are two types of chirp signals in general: linear chirp where frequency changes linearly with time and exponential chirp whose frequency varies with time exponentially. Chirp signals have been mainly used in SONAR and radar systems. In [1] chirp signal is used in sub-bottom profilers to penetrate the shallow-water subsurface layers. Compared to single frequency (monotonic) signals, chirp signals provide better range resolution at the output of the matched filter [1]. Other applications of chirp signals are in spread spectrum communication systems, ultrashort laser pulses, etc. Some applications of chirp signals in underwater communication can be found in [2] and [3]. A linear chirp signal is employed in [2] for time acquisition in underwater acoustic orthogonal frequency division multiplexing (OFDM) systems. Improvement of time synchronization performance is observed due to the sharp peak at the matched filter output of the linear frequency modulation (LFM) signal. The possibility of increasing spectral efficiency by employing exponential chirp signals is discussed in [3].

Underwater acoustic communication in particle velocity channels using vector transducers is an emerging area of research and development. A vector communication system is composed of vector transducers, i.e., sensors and/or projectors, which measure or stimulate, respectively, the particle velocity components of the acoustic field. In [4] and [5], a compact multichannel receiver/equalizer is proposed and studied, where the vector sensor receiver measures the signal in the pressure channel, as well as the y and z particle velocity channels. All these channels are measured at a single point in space by a compact vector sensor. Data transmission using vector projectors is investigated in [6] and [7]. More specifically, a method is proposed in there for data modulation in particle velocity channels using transmit dipoles.

Channel correlations in space, frequency and time domains are derived in [8] and [9] for an array of vector sensor communication receivers. Delay and Doppler spreads of acoustic particle velocity communication channels are calculated in [9] using channel zero crossing rates obtained from frequency and temporal correlation functions, respectively. Characterization of acoustic particle velocity and acceleration channels in communication systems is studied in [6], [7], [10], where the transmitters and the receivers are vector projectors and vector sensors, respectively. At-sea experiments for coherent communication and data reception using an array of vector sensors are reported in [11]. Measured narrowband and wideband capacities of acoustic particle velocity channels in the ocean are presented in [12], as well as some channel statistics such as channel amplitude distributions, channel temporal correlations and power delay profiles. The OFDM

capacity of a vector sensor communication receiver which measures the particle velocity and acoustic pressure is studied in [13].

In this paper, performance of an underwater acoustic vector sensor receiver with LFM is analyzed. The rest of paper is organized as follows: system equations are presented in Section II, channel and noise covariance matrices are derived in Section III, simulation results and system performance are discussed in Section IV and concluding remarks are provided in Section V.

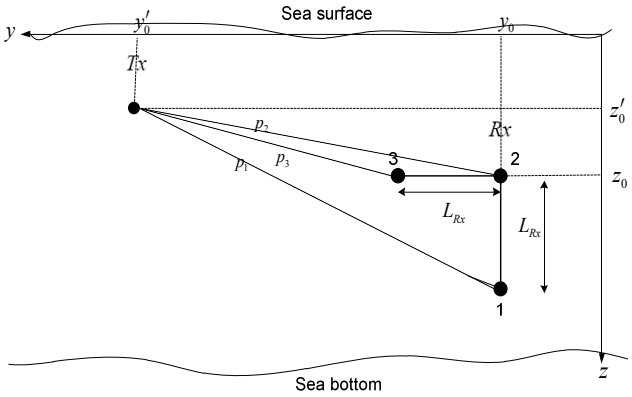

Fig. 1. A 1×3 single-input multiple-output underwater acoustic communication system in shallow water. Transmitter is a scalar projector and receiver is a vector sensor composed of two dipoles which measure the *y* and *z* components of acoustic particle velocity.

II. System Description and Equations

In range-depth *y*-*z* plane, an acoustic vector sensor receiver system is shown in Fig. 1, where there is one scalar projector and a vector sensor receiver measuring signals in pressure and *y* and *z* particle velocity channels. Inside the vector sensor receiver there are three scalar sensors, labeled as 1, 2 and 3. Define the pressure channel response from *Tx* to the three scalar sensors at *Rx* as p_1, p_2 and p_3, where the spacing between sensors 1 and 2 and also 2 and 3 is L_{Rx}. When L_{Rx} is small enough, then according to the definition of particle velocity channels [4], *y* and *z* pressure-equivalent particle velocity channels in Fig. 1 can be written as

$$\begin{aligned} p_y &= (jkL_{Rx})^{-1}(p_3 - p_2), \\ p_z &= (jkL_{Rx})^{-1}(p_1 - p_2), \end{aligned} \tag{1}$$

where $j = \sqrt{-1}$, $k = 2\pi/\lambda$ is the wave number and $\lambda = c/f_0$ is the wavelength.

A linear chirp signal is given by [2]

$$s(t) = A\cos(\omega_0 t + 0.5\beta t^2), \quad 0 \le t \le T, \tag{2}$$

where A is the amplitude, $\omega_0 = 2\pi f_0$ and f_0 is the carrier frequency, $\beta = 2\pi B/T$ is the frequency rate, B is the chirp signal bandwidth and T is the signal duration. This signal exhibits sharp ambiguity in time domain and approximate rectangular amplitude in frequency domain.

If T is large enough to include all the multipath delays in the acoustic underwater channel, then we can model the channel as a frequency-flat fading channel. Therefore, system equations for the 1×3 single-input-multiple-output (SIMO) system in Fig. 1 can written as

$$\begin{bmatrix} r_2(t) \\ r_y(t) \\ r_z(t) \end{bmatrix} = \begin{bmatrix} p_2 \\ p_y \\ p_z \end{bmatrix} x(t) + \begin{bmatrix} n_2(t) \\ n_y(t) \\ n_z(t) \end{bmatrix}. \tag{3}$$

Here $x(t)$ is a sequence of chirp signals given in (2), p_2 is the Rayleigh flat-fading pressure channel response, and p_y and p_z are Rayleigh flat-fading pressure-equivalent velocity channel responses in *y* and *z* directions, respectively, as defined in (1). The Rayleigh fading model is used because it is shown in [12] that Rayleigh distribution fits closely to the measured particle velocity and pressure channel responses. Note that r_2 and n_2 are the received signal and ambient noise pressure at the scalar sensor 2 in Fig. 1, whereas r_y and r_z are the received signals measured by the horizontal and vertical dipoles, respectively, and n_y and n_z are the *y* and *z* components of the pressure-equivalent ambient noise velocity, respectively.

III. Noise and Channel Covariance Matrices

Consider that the ambient noise is composed of two components: surface-generated noise and an isotropic component caused by miscellaneous factors [14]. Using a parametric angular probability density function (PDF) [15] for the surface-generated noise, the noise angle-of-arrival (AOA) PDF can be written as

$$g_\Theta(\theta) = \Delta\frac{\exp[\nu\cos(\theta-\theta_p)]}{2\pi I_0(\nu)} + (1-\Delta)\frac{1}{2\pi}, \tag{4}$$

where Θ is the noise AOA measured with respect to the positive *y* axis counterclockwise, $0 < \Delta < 1$ denotes the proportion of the surface-generated noise component, ν is inversely related to the surface-generated noise angular width, θ_p represents the peak angle of the PDF and $I_m(\cdot)$ is the *m*-th order modified Bessel function of the first kind. Close agreement of the proposed noise AOA model in (4) with experimental data is shown in Section IV. Compared to the noise AOA PDFs in [14], the parametric form of (4) makes it adaptable to various sea conditions. Moreover, as shown in what follows and also in the Appendix, it provides closed-form analytical correlation expressions that are

suitable for calculating the noise covariance matrix of the proposed vector sensor communication receiver [4] [5] in Fig. 1.

Following the same approach as [15], spatial correlation of the ambient noise pressure field between the points (y_0, z_0) and $(y_0+\varepsilon_y, z_0+L)$ in the range-depth plane can be written as

$$q_n(L,\varepsilon_y) = E_\Theta[\exp(jk\sqrt{L^2+\varepsilon_y^2}\cos(\Theta-\theta_0)], \quad (5)$$

where $E[.]$ is the mathematical expectation and $\theta_0 = \tan^{-1}(L/\varepsilon_y)$. Using (18) in [15] and the PDF in (4), this expectation can be solved which results in the following closed-form expression for the spatial correlation of the ambient noise pressure field

$$q_n(L,\varepsilon_y) = (1-\Delta)J_0(k\sqrt{L^2+\varepsilon_y^2}) + \Delta\frac{J_0(j\sqrt{\nu^2-k^2(L^2+\varepsilon_y^2)+j2\nu k(\cos(\theta_p)\varepsilon_y+\sin(\theta_p)L)})}{J_0(j\nu)}, \quad (6)$$

where $J_m(\cdot)$ is m-th order Bessel function of the first kind such that $I_m(x) = j^{-m}J_m(jx)$. With $\Delta = 0$, (6) simplifies to the isotropic noise considered in the acoustic vector transducer-based underwater communication systems developed in [4]-[7].

For the 1×3 SIMO system with a vector sensor receiver in Fig. 1, the covariance matrix of the noise components in (3) is given by

$$\Sigma_{vector} = E\left[\begin{bmatrix} n_2 \\ n_y \\ n_z \end{bmatrix}[n_2^* \; n_y^* \; n_z^*]\right] = \begin{bmatrix} 1 & E[n_2 n_y^*] & E[n_2 n_z^*] \\ E[n_y n_2^*] & \Omega_y^n & E[n_y n_z^*] \\ E[n_z n_2^*] & E[n_z n_y^*] & \Omega_z^n \end{bmatrix}, \quad (7)$$

where * is the complex conjugate. Closed-form expressions for the terms $E[n_2 n_z^*]$, $E[n_2 n_y^*]$, Ω_z^n, Ω_y^n and $E[n_y n_z^*]$ are given in (21)-(25), respectively, derived in the Appendix using (6) and its derivatives.

In a system where the sensor pairs {1,2} and {2,3} in Fig. 1 are not utilized as dipoles, to measure the y and z components of acoustic particle velocity, we have a fully scalar 1×3 SIMO system with the following system equations

$$\begin{bmatrix} r_1(t) \\ r_2(t) \\ r_3(t) \end{bmatrix} = \begin{bmatrix} p_1 \\ p_2 \\ p_3 \end{bmatrix} x(t) + \begin{bmatrix} n_1(t) \\ n_2(t) \\ n_3(t) \end{bmatrix}. \quad (8)$$

The noise covariance matrix for this system is given by

$$\Sigma_{scalar} = E\left[\begin{bmatrix} n_1 \\ n_2 \\ n_3 \end{bmatrix}[n_1^* \; n_2^* \; n_3^*]\right] = \begin{bmatrix} 1 & q_n(-L_{Rx},0) & q_n(-L_{Rx},L_{Rx}) \\ q_n^*(-L_{Rx},0) & 1 & q_n(0,L_{Rx}) \\ q_n^*(-L_{Rx},L_{Rx}) & q_n^*(0,L_{Rx}) & 1 \end{bmatrix}, \quad (9)$$

where $q_n(.,.)$ is given in (6). The elements of this covariance matrix can therefore be written as

$$\begin{aligned} q_n(-L_{Rx},0) &= (1-\Delta)J_0(kL_{Rx}) + \Delta\frac{J_0(j\sqrt{\nu^2-k^2L_{Rx}^2-j2\nu k\sin(\theta_p)L_{Rx}})}{J_0(j\nu)}, \\ q_n(-L_{Rx},L_{Rx}) &= (1-\Delta)J_0(k\sqrt{2}L_{Rx}) + \Delta\frac{J_0(j\sqrt{\nu^2-2k^2L_{Rx}^2+j2\nu k(\cos(\theta_p)-\sin(\theta_p))L_{Rx}})}{J_0(j\nu)}, \\ q_n(0,L_{Rx}) &= (1-\Delta)J_0(kL_{Rx}) + \Delta\frac{J_0(j\sqrt{\nu^2-k^2L_{Rx}^2+j2\nu k\cos(\theta_p)L_{Rx}})}{J_0(j\nu)}. \end{aligned} \quad (10)$$

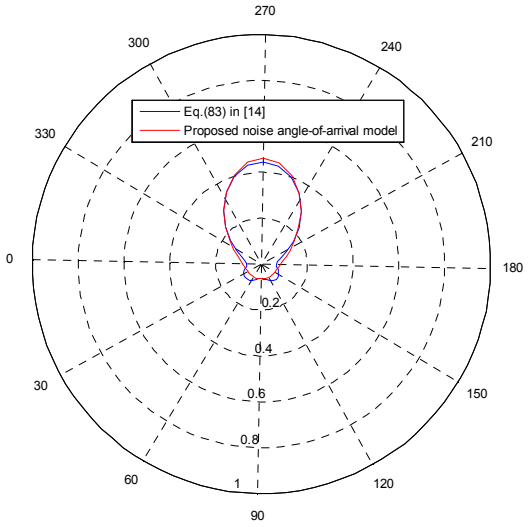

Fig. 2. Polar plot of the proposed ambient noise AOA model, compared with the experimentally-verified noise AOA in [14].

In addition to the noise covariance matrices, one needs to consider channel covariance matrices of the two systems in (3) and (8) as well. Here we use the shallow water channel representation [8] where rays are received around the mean AOAs μ_b and μ_s from the sea bottom and surface, respectively. Additionally, σ_b and σ_s are standard deviations of the AOAs from the bottom and surface,

respectively, and $0 \le \Lambda_b \le 1$ represents the proportion of arriving rays coming from the sea bottom. Using the particle velocity and pressure channel correlations derived in [8], the channel covariance matrix for the 1×3 SIMO vector receiver system in (3) can be written as

$$\mathbf{C}_{vector} = E\left[\begin{bmatrix} p_2 \\ p_y \\ p_z \end{bmatrix}[p_2^* \;\; p_y^* \;\; p_z^*]\right] =$$

$$\begin{bmatrix} 1 & \Lambda_b\cos(\mu_b)+(1-\Lambda_b)\cos(\mu_s) & \Lambda_b\sin(\mu_b)+(1-\Lambda_b)\sin(\mu_s) \\ \Lambda_b\cos(\mu_b)+(1-\Lambda_b)\cos(\mu_s) & \Lambda_b(\cos^2(\mu_b)+\sigma_b^2\sin^2(\mu_b))+(1-\Lambda_b)(\cos^2(\mu_s)+\sigma_s^2\sin^2(\mu_s)) & \Lambda_b(1-\sigma_b^2)\times\cos(\mu_b)\sin(\mu_b)+(1-\Lambda_b)(1-\sigma_s^2)\times\cos(\mu_s)\sin(\mu_s) \\ \Lambda_b\sin(\mu_b)+(1-\Lambda_b)\sin(\mu_s) & \Lambda_b(1-\sigma_b^2)\times\cos(\mu_b)\sin(\mu_b)+(1-\Lambda_b)(1-\sigma_s^2)\times\cos(\mu_s)\sin(\mu_s) & \Lambda_b(\sin^2(\mu_b)+\sigma_b^2\cos^2(\mu_b))+(1-\Lambda_b)(\sin^2(\mu_s)+\sigma_s^2\cos^2(\mu_s)) \end{bmatrix} \quad (11)$$

On the other hand, based upon the pressure channel spatial correlation derived in [8], the channel covariance matrix for the 1×3 SIMO scalar receiver system in (8) can be shown to be

$$\mathbf{C}_{scalar} = E\left[\begin{bmatrix} p_1 \\ p_2 \\ p_3 \end{bmatrix}[p_1^* \;\; p_2^* \;\; p_3^*]\right] = \begin{bmatrix} 1 & \rho_{12} & \rho_{13} \\ \rho_{12}^* & 1 & \rho_{23} \\ \rho_{13}^* & \rho_{23}^* & 1 \end{bmatrix}, \quad (12)$$

where the matrix elements are

$$\rho_{12} = \Lambda_b \exp(-jkL_{Rx}\sin(\mu_b))\exp(-0.5\sigma_b^2k^2(L_{Rx}\cos(\mu_b))^2) + (1-\Lambda_b)\exp(-jkL_{Rx}\sin(\mu_s))\exp(-0.5\sigma_s^2k^2(L_{Rx}\cos(\mu_s))^2),$$

$$\rho_{13} = \Lambda_b \exp(jkL_{Rx}(\cos(\mu_b)-\sin(\mu_b)))\exp(-0.5\sigma_b^2k^2 \times(L_{Rx}\cos(\mu_b)-L_{Rx}\sin(\mu_b))^2) + (1-\Lambda_b)\exp(jkL_{Rx}(\cos(\mu_s)-\sin(\mu_s)))\exp(-0.5\sigma_s^2k^2 \times(L_{Rx}\cos(\mu_s)-L_{Rx}\sin(\mu_s))^2),$$

$$\rho_{23} = \Lambda_b \exp(jkL_{Rx}\cos(\mu_b))\exp(-0.5\sigma_b^2k^2(L_{Rx}\sin(\mu_b))^2) + (1-\Lambda_b)\exp(jkL_{Rx}\cos(\mu_s))\exp(-0.5\sigma_s^2k^2(L_{Rx}\sin(\mu_s))^2). \quad (13)$$

IV. Simulation Setup and Performance Analysis

For simulations and system performance analysis, the noise AOA model parameters are obtained by fitting eq. (4) to the experimentally verified noise AOA PDF provided in eq. (83) of [14]. Fig. 2 exhibits the noise AOA PDF given in eq. (83) of [14], together with the proposed model in (4), such that $\Delta = 0.6$, $\nu = 3.076$ and $\theta_p = 270^\circ$. We observe that the proposed model is close enough to the data of [14].

To compute channel correlations, we have considered these channel parameters: $\sigma_s = 1.5^\circ$, $\sigma_b = 2^\circ$, $\mu_b = \pi/18\ (10^\circ)$, $\mu_s = 348\pi/180\ (348^\circ)$ and $\Lambda_b = 0.4$. Other parameters in the simulations are the sound speed $c = 1500$m/s, $f_0 = 12$ kHz, and $\beta = 2\times 10^6$ and $T = 20$ ms for the chirp signal.

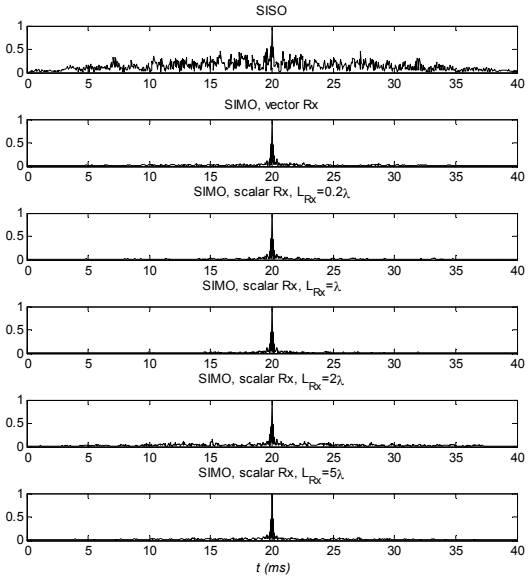

Fig. 3. The matched filter output of the LFM chirp signal in three systems with SNR = 5 dB. There is a single scalar transmitter in all systems. In the SISO system at the top panel the receiver is a single scalar sensor. In the second panel the 1×3 SIMO system has the vector sensor receiver of Fig. 1 with L_{Rx} = 0.2λ, which measures the acoustic pressure, as well as the y and z components of acoustic particle velocity. The last four panels are for a 1×3 SIMO system which has a receive array of three scalar sensors arranged similarly to Fig. 1. These four panels correspond to L_{Rx} = 0.2λ, λ, 2λ, and 5λ, respectively.

When the channel coefficients in (3) are known perfectly at the receiver, the output of a maximal ratio combiner (MRC) fed by the vector sensor signals can be written as

$$\xi(t) = (|p_2|^2 + |p_y|^2 + |p_z|^2)^{-1}[p_2^* \;\; p_y^* \;\; p_z^*]\begin{bmatrix} r_2(t) \\ r_y(t) \\ r_z(t) \end{bmatrix}$$
$$= x(t) + (|p_2|^2 + |p_y|^2 + |p_z|^2)^{-1}(p_2^*n_2(t) + p_y^*n_y(t) + p_z^*n_z(t)). \quad (14)$$

The output of the LFM chirp matched filter, with $\xi(t)$ in (14) at its input is given by

$$\zeta(t) = \xi(t) \otimes s^*(-t), \tag{15}$$

where $\otimes$ stands for convolution.

With a normalized $s(t)$, $A = 1$ in (2), the matched filter output after the MRC is plotted in Fig.3. Three different receivers are simulated in Fig. 3: (a) a single-input single-output (SISO) system with one scalar transmitter and one scalar receiver, (b) the proposed 1×3 SIMO system in Fig. 1 with one scalar transmitter and a vector sensor receiver with $L_{Rx} = 0.2\lambda$ whose MRC/matched filter output signal is $\zeta(t)$ in (15), and (c) a 1×3 SIMO fully scalar system which has a receive array of three scalar sensors arranged similarly to Fig. 1, with multiple values for L_{Rx}. The MRC/matched filter output signal for this system is similar to (14) and (15), where p_y, p_z, r_y, r_z, n_y and n_z are replaced by p_1, p_3, r_1, r_3, n_1 and n_3.

According to Fig. 3, the SIMO vector sensor matched filter has an output peak sharper than the SISO scalar matched filter. The output of the vector sensor matched filter has much less fluctuations as well. Performance of the SIMO scalar matched filter depends on its element spacing. As L_{Rx} increases, the output peak becomes sharper and fluctuations reduce. This is at the cost of a larger receiver, whereas the compact vector sensor receiver has a small size, as it measures the acoustic pressure and y and z particle velocities at a single point in space.

To quantify the matched filter performance, we use the peak-to-average ratio (PAR) of the matched filter output as the metric. If $\zeta(t)$ is the matched filter output signal, then its PAR is defined by $\zeta_{\text{PAR}} = |\zeta(t)|_{peak} / \zeta_{rms}$, where $|\zeta(t)|_{peak}$ denotes the peak value of $\zeta(t)$'s absolute value and $\zeta_{rms} = \{T^{-1}\int_0^T \zeta^2(t)dt\}^{1/2}$ is the root-mean-squared value of $\zeta(t)$. The PAR factors of the three chirp LFM matched filter systems are plotted in Fig. 4 versus the average signal-to-noise ratio (SNR) per channel. All the channel and noise powers are normalized to 1 and each curve is obtained by averaging over 100 symbols.

As shown in Fig. 4, the vector sensor LFM chirp system outperforms the conventional LFM chirp system with a single hydrophone. The SNR saving offered by the vector sensor receiver is about 7 dB, compared to the single scalar receiver. This is particularly important for detection, acquisition and synchronization in underwater acoustic communication systems operating at low SNRs. The PAR performance of the system with three scalar receivers depends on the element spacing L_{Rx}. Typically by increasing L_{Rx} the performance of the fully scalar receiver may improve, although this increases its size as well. This may not be acceptable for platforms with serious size limitations such as small autonomous underwater vehicles.

The performance of the SIMO vector sensor LFM receiver is significantly better, about 4.5 dB in Fig. 4, compared to the fully scalar SIMO LFM receiver with the small element spacing of $L_{Rx} = 0.2\lambda$. To understand this, absolute values of the noise and channel covariance matrices are provided in (16). Comparison of the noise covariance matrices Σ_{vector} and $\Sigma_{scalar,0.2\lambda}$ reveals that the noise components are less correlated in the vector sensor receiver. More specifically, the p and y noise components in the vector sensor are uncorrelated due to the vertical direction of the surface-generated noise. This is obtained by plugging $\theta_p = 270^\circ$ into (23). This is while the correlation between n_1 and n_2 in the fully scalar receiver is 0.73. Additionally, y and z vector sensor noises are uncorrelated according to (26), whereas the correlation between n_2 and n_3 in the fully scalar receiver is 0.74.

$$\text{magnitudes of } \Sigma_{vector} = \begin{bmatrix} 1 & 0 & 0.61111 \\ 0 & 1 & 0 \\ 0.6111 & 0 & 1 \end{bmatrix},$$

$$\text{magnitudes of } \Sigma_{scalar,0.2\lambda} = \begin{bmatrix} 1 & 0.7347 & 0.5465 \\ 0.7347 & 1 & 0.7404 \\ 0.5465 & 0.7404 & 1 \end{bmatrix},$$

$$\text{magnitudes of } \Sigma_{scalar,2\lambda} = \begin{bmatrix} 1 & 0.3299 & 0.1074 \\ 0.3299 & 1 & 0.0731 \\ 0.1074 & 0.0731 & 1 \end{bmatrix},$$

$$\text{magnitudes of } \Sigma_{scalar,5\lambda} = \begin{bmatrix} 1 & 0.2093 & 0.105 \\ 0.2093 & 1 & 0.0498 \\ 0.105 & 0.0498 & 1 \end{bmatrix},$$

$$\text{magnitudes of } \mathbf{C}_{vector} = \begin{bmatrix} 1 & 1 & 0.0924 \\ 1 & 1 & 0.0985 \\ 0.0924 & 0.0985 & 1 \end{bmatrix},$$

$$\text{magnitudes of } \mathbf{C}_{scalar,0.2\lambda} = \begin{bmatrix} 1 & 0.9586 & 0.9564 \\ 0.9586 & 1 & 0.9999 \\ 0.9564 & 0.9999 & 1 \end{bmatrix},$$

$$\text{magnitudes of } \mathbf{C}_{scalar,2\lambda} = \begin{bmatrix} 1 & 0.9302 & 0.9420 \\ 0.9302 & 1 & 0.9943 \\ 0.9420 & 0.9943 & 1 \end{bmatrix},$$

$$\text{magnitudes of } \mathbf{C}_{scalar,5\lambda} = \begin{bmatrix} 1 & 0.3827 & 0.3352 \\ 0.3827 & 1 & 0.9650 \\ 0.3352 & 0.9650 & 1 \end{bmatrix}. \tag{16}$$

Another factor that can contribute to the performance of gain of the vector sensor LFM receiver over the fully scalar receiver with $L_{Rx} = 0.2\lambda$ is the channel covariance matrix. In the vector sensor channel covariance matrix $\mathbf{C}_{vector}$ in (16) we observe the channel pairs $\{p_2, p_z\}$ and $\{p_y, p_z\}$ are

uncorrelated. However, the corresponding channel pairs $\{p_1, p_3\}$ and $\{p_2, p_3\}$ in the fully scalar receiver are highly correlated, according to the channel covariance matrix $\mathbf{C}_{scalar,0.2\lambda}$ in (16).

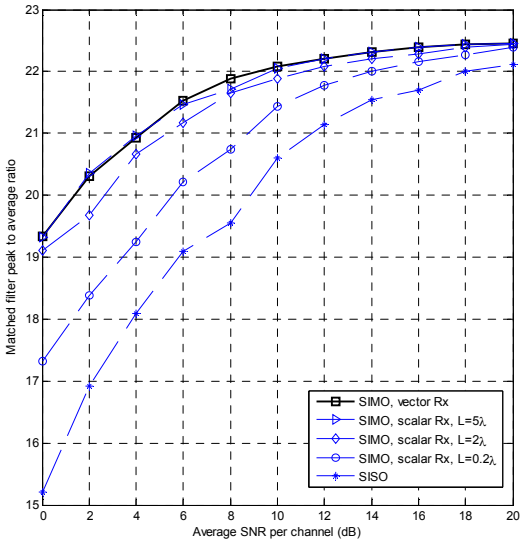

Fig. 4. Peak-to-average ratio of the LFM chirp match filter in three systems: SIMO with a vector sensor receiver, SIMO with three scalar receivers, L_{Rx} = 0.2λ, 2λ, 5λ, and SISO with a single scalar receiver.

V. Conclusion

In this paper, chirp linear frequency modulation is studied in underwater communication systems with acoustic vector sensors as receivers. A vector sensor is capable of measuring the particle velocity components of the acoustic field, in addition to the acoustic pressure. A parametric noise model for the vector sensor receiver is developed which provides closed-form expressions for possible correlations among the vector and scalar components of the ambient noise field. Using the derived noise and channel covariance matrices, the output of a vector sensor matched to a chirp signal is calculated and compared with a standard scalar matched filter. It is observed that the vector matched filter provides a sharper peak at the output and significantly suppresses the noise. For example, for the considered channel and noise parameters, the proposed vector sensor chirp matched filter offers a 7 dB SNR saving, compared to a single scalar chirp matched filter. For low SNR signal acquisition and synchronization, this gain is particularly important. This is while the multi-channel vector sensor communication receiver has a compact size, as it measures the vector and scalar components of the acoustic field all at a single point in space. This makes the vector sensor receiver specially suitable for small autonomous or unmanned underwater vehicles, or other small platforms.

Appendix

Ambient Noise Particle Velocity and Pressure Correlations in a Vector Sensor Receiver

According to the definition of pressure-equivalent particle velocity [4] [8], the spatial correlation between the pressure and pressure-equivalent particle velocity ambient noise components can be obtained by taking the derivatives of $q_n(L,\varepsilon_y)$, the pressure noise spatial correlation, with respect to L and ε_y, the vertical and horizontal displacements, respectively. The results are given in (17) and (18)

$$
\begin{aligned}
&(jk)^{-1}\partial q_n(L,\varepsilon_y)/\partial L = \\
&\Delta\frac{J_1(j\sqrt{\nu^2-k^2(L^2+\varepsilon_y^2)+j2\nu k(\cos(\theta_p)\varepsilon_y+\sin(\theta_p)L)}\,)}{J_0(j\nu)} \\
&\times\frac{kL-j\nu\sin(\theta_p)}{\sqrt{\nu^2-k^2(L^2+\varepsilon_y^2)+j2\nu k(\cos(\theta_p)\varepsilon_y+\sin(\theta_p)L)}} \\
&+(1-\Delta)J_1(k\sqrt{L^2+\varepsilon_y^2})\frac{jL}{\sqrt{L^2+\varepsilon_y^2}},
\end{aligned}
\tag{17}
$$

$$
\begin{aligned}
&(jk)^{-1}\partial q_n(L,\varepsilon_y)/\partial \varepsilon_y = \\
&\Delta\frac{J_1(j\sqrt{\nu^2-k^2(L^2+\varepsilon_y^2)+j2\nu k(\cos(\theta_p)\varepsilon_y+\sin(\theta_p)L)}\,)}{J_0(j\nu)} \\
&\times\frac{k\varepsilon_y-j\nu\cos(\theta_p)}{\sqrt{\nu^2-k^2(L^2+\varepsilon_y^2)+j2\nu k(\cos(\theta_p)\varepsilon_y+\sin(\theta_p)L)}} \\
&+(1-\Delta)J_1(k\sqrt{L^2+\varepsilon_y^2})\frac{j\varepsilon_y}{\sqrt{L^2+\varepsilon_y^2}}.
\end{aligned}
\tag{18}
$$

Similarly to [4] and [8], the spatial correlation between the y and z pressure-equivalent particle velocity noise components can be calculated by taking the second derivatives of $q_n(L,\varepsilon_y)$ with respect to L and ε_y. The results are provided in (19) - (21).

Since the vector sensor receiver measures the signal in pressure and particle velocity channels all at a single point in space, correlations among the three noise terms in (3) and their powers can be obtained by letting $L\to 0$ and $\varepsilon_y \to 0$ in (22) - (26). With $\Delta = 0$, (22), (23) and (26) reduce to zero, i.e., no correlation between the vector sensor noise components in (3). This refers to the isotropic ambient noise model for the vector sensor communication receiver in [4] and [5], as well as other vector transducer-based underwater

communication systems in [6] and [7] which have a vector projector at the transmit side.

$$-k^{-2}\partial^2 q_n(L,\varepsilon_y)/\partial L^2 =$$
$$\Delta\left\{\frac{1}{2}\left(\frac{J_0(j\sqrt{\nu^2-k^2(L^2+\varepsilon_y^2)+j2\nu k(\cos(\theta_p)\varepsilon_y+\sin(\theta_p)L)}\,)}{J_0(j\nu)}\right.\right.$$
$$\left.\left.-\frac{J_2(j\sqrt{\nu^2-k^2(L^2+\varepsilon_y^2)+j2\nu k(\cos(\theta_p)\varepsilon_y+\sin(\theta_p)L)}\,)}{J_0(j\nu)}\right)\right.$$
$$\times\frac{-(kL-j\nu\sin(\theta_p))^2}{\nu^2-k^2(L^2+\varepsilon_y^2)+j2\nu k(\cos(\theta_p)\varepsilon_y+\sin(\theta_p)L)}$$
$$+\frac{J_1(j\sqrt{\nu^2-k^2(L^2+\varepsilon_y^2)+j2\nu k(\cos(\theta_p)\varepsilon_y+\sin(\theta_p)L)}\,)}{J_0(j\nu)}$$
$$\times\left(\frac{-j}{\sqrt{\nu^2-k^2(L^2+\varepsilon_y^2)+j2\nu k(\cos(\theta_p)\varepsilon_y+\sin(\theta_p)L)}}\right.$$
$$\left.\left.-j\frac{(kL-j\nu\sin(\theta_p))^2}{(\nu^2-k^2(L^2+\varepsilon_y^2)+j2\nu k(\cos(\theta_p)\varepsilon_y+\sin(\theta_p)L))^{3/2}}\right)\right\}$$
$$+(1-\Delta)\left\{\frac{1}{2}\left(J_0(k\sqrt{L^2+\varepsilon_y^2})-J_2(k\sqrt{L^2+\varepsilon_y^2})\right)\frac{\varepsilon_y^2}{L^2+\varepsilon_y^2}\right.$$
$$\left.+J_1(k\sqrt{L^2+\varepsilon_y^2})\frac{L^2}{k(L^2+\varepsilon_y^2)^{3/2}}\right\},\tag{19}$$

$$-k^{-2}\partial^2 q_n(L,\varepsilon_y)/\partial \varepsilon_y^2 =$$
$$\Delta\left\{\frac{1}{2}\left(\frac{J_0(j\sqrt{\nu^2-k^2(L^2+\varepsilon_y^2)+j2\nu k(\cos(\theta_p)\varepsilon_y+\sin(\theta_p)L)}\,)}{J_0(j\nu)}\right.\right.$$
$$\left.\left.-\frac{-J_2(j\sqrt{\nu^2-k^2(L^2+\varepsilon_y^2)+j2\nu k(\cos(\theta_p)\varepsilon_y+\sin(\theta_p)L)}\,)}{J_0(j\nu)}\right)\right.$$
$$\times\frac{-(k\varepsilon_y-j\nu\cos(\theta_p))^2}{\nu^2-k^2(L^2+\varepsilon_y^2)+j2\nu k(\cos(\theta_p)\varepsilon_y+\sin(\theta_p)L)}$$
$$+\frac{J_1(j\sqrt{\nu^2-k^2(L^2+\varepsilon_y^2)+j2\nu k(\cos(\theta_p)\varepsilon_y+\sin(\theta_p)L)}\,)}{J_0(j\nu)}$$
$$\times\left(\frac{-j}{\sqrt{\nu^2-k^2(L^2+\varepsilon_y^2)+j2\nu k(\cos(\theta_p)\varepsilon_y+\sin(\theta_p)L)}}\right.$$
$$\left.\left.-j\frac{(k\varepsilon_y-j\nu\cos(\theta_p))^2}{(\nu^2-k^2(L^2+\varepsilon_y^2)+j2\nu k(\cos(\theta_p)\varepsilon_y+\sin(\theta_p)L))^{3/2}}\right)\right\}$$
$$+(1-\Delta)\left\{\frac{1}{2}(J_0(k\sqrt{L^2+\varepsilon_y^2})-J_2(k\sqrt{L^2+\varepsilon_y^2}))\frac{\varepsilon_y^2}{L^2+\varepsilon_y^2}\right.$$
$$\left.+J_1(k\sqrt{L^2+\varepsilon_y^2})\frac{L^2}{k(L^2+\varepsilon_y^2)^{3/2}}\right\},\tag{20}$$

$$-k^{-2}\partial^2 q_n(L,\varepsilon_y)/\partial L\partial \varepsilon_y =$$
$$\Delta\left\{\frac{1}{2}\left(\frac{J_0(j\sqrt{\nu^2-k^2(L^2+\varepsilon_y^2)+j2\nu k(\cos(\theta_p)\varepsilon_y+\sin(\theta_p)L)}\,)}{J_0(j\nu)}\right.\right.$$
$$\left.\left.-\frac{-J_2(j\sqrt{\nu^2-k^2(L^2+\varepsilon_y^2)+j2\nu k(\cos(\theta_p)\varepsilon_y+\sin(\theta_p)L)}\,)}{J_0(j\nu)}\right)\right.$$
$$\times\frac{-(k\varepsilon_y-j\nu\cos(\theta_p))(kL-j\nu\sin(\theta_p))}{\nu^2-k^2(L^2+\varepsilon_y^2)+j2\nu k(\cos(\theta_p)\varepsilon_y+\sin(\theta_p)L)}$$
$$+\frac{J_1(j\sqrt{\nu^2-k^2(L^2+\varepsilon_y^2)+j2\nu k(\cos(\theta_p)\varepsilon_y+\sin(\theta_p)L)}\,)}{J_0(j\nu)}$$
$$\times\left.\left(-j\frac{(k\varepsilon_y-j\nu\cos(\theta_p))(kL-j\nu\sin(\theta_p))}{(\nu^2-k^2(L^2+\varepsilon_y^2)+j2\nu k(\cos(\theta_p)\varepsilon_y+\sin(\theta_p)L))^{3/2}}\right)\right\}$$
$$+(1-\Delta)\left\{\frac{1}{2}(J_0(k\sqrt{L^2+\varepsilon_y^2})-J_2(k\sqrt{L^2+\varepsilon_y^2}))\frac{L\varepsilon_y}{L^2+\varepsilon_y^2}\right.$$
$$\left.-J_1(k\sqrt{L^2+\varepsilon_y^2})\frac{L\varepsilon_y}{k(L^2+\varepsilon_y^2)^{3/2}}\right\}.\tag{21}$$

$$E[n_2 n_z^*]=(jk)^{-1}\partial q_n(L,0)/\partial L\big|_{L=0}=-j\Delta\frac{J_1(j\nu)}{J_0(j\nu)}\sin\theta_p,\tag{22}$$

$$E[n_2 n_y^*]=(jk)^{-1}\partial q_n(0,\varepsilon_y)/\partial \varepsilon_y\big|_{\varepsilon_y=0}=-j\Delta\frac{J_1(j\nu)}{J_0(j\nu)}\cos\theta_p,\tag{23}$$

$$\Omega_z^n=E[|\,n_z\,|^2]=-k^{-2}\partial^2 q_n(L,0)/\partial L^2\big|_{L=0}$$
$$=\Delta\left\{\frac{1}{2}\frac{J_0(j\nu)-J_2(j\nu)}{J_0(j\nu)}\sin^2\theta_p+\frac{j(\sin^2(\theta_p)-1)}{\nu}\frac{J_1(j\nu)}{J_0(j\nu)}\right\}$$
$$+\frac{1-\Delta}{2},\tag{24}$$

$$\Omega_y^n=E[|\,n_y\,|^2]=-k^{-2}\partial^2 q_n(0,\varepsilon_y)/\partial \varepsilon_y^2\big|_{\varepsilon_y=0}$$
$$=\Delta\left\{\frac{1}{2}\frac{J_0(j\nu)-J_2(j\nu)}{J_0(j\nu)}\cos^2\theta_p+\frac{j(\cos^2(\theta_p)-1)}{\nu}\frac{J_1(j\nu)}{J_0(j\nu)}\right\}$$
$$+\frac{1-\Delta}{2},\tag{25}$$

$$E[n_y n_z^*]=-k^{-2}\partial^2 q_n(L,\varepsilon_y)/\partial L\partial \varepsilon_y\big|_{L=\varepsilon_y=0}$$
$$=\Delta\left\{\frac{1}{2}\frac{J_0(j\nu)-J_2(j\nu)}{J_0(j\nu)}\sin\theta_p\cos\theta_p+\frac{j\sin\theta_p\cos\theta_p}{\nu}\frac{J_1(j\nu)}{J_0(j\nu)}\right\}.\tag{26}$$

REFERENCES

[1] D. Tang and B. T. Hefner, " Modeling interface roughness scattering in a layered seabed for normal-incident chirp sonar signals," *J. Acoust. Soc. Am.*, vol. 131, pp. EL302-EL308, 2012.

[2] W. Wei, X. Hu, D. Wang, R. Xu and H. Sun, "Performance comparison of time synchronization algorithms for OFDM underwater communication system," in *Proc. 14th Int. Conf. on Mechatronics and Machine Vision in Practice*, Xiamen, China, 2007, pp.104-107.

[3] P. Courmontagne, G. Fages and P. P. Beaujean, "A chirp FSK improvement for communications in shallow water using bandwidth overlapping," in *Proc. Oceans*, Quebec City, QC, Canada, 2008, pp.1-7.

[4] A. Abdi and H. Guo, "A new compact multichannel receiver for underwater wireless communication networks," *IEEE Trans. Wireless Commun.*, vol. 8, pp. 3326-3329, 2009.

[5] A. Abdi, H. Guo and P. Sutthiwan, "A new vector sensor receiver for underwater acoustic communication," in *Proc. Oceans*, Vancouver, BC, Canada, 2007, pp. 1-10.

[6] C. Chen and A. Abdi, "Underwater communication in acoustic particle velocity channels via vector transducers," in *Proc. Conf. on Underwater Communications: Channel Modelling and Validation*, Sestri Levante, Italy, 2012.

[7] C. Chen and A. Abdi, "Utilization of underwater particle velocity channels for data transmission: Signals, channels and system performance," in *Proc. IEEE Int. Conf. Commun.*, Ottawa, ON, Canada, 2012, pp. 1-5.

[8] A. Abdi and H. Guo, "Signal correlation modeling in acoustic vector sensor arrays," *IEEE Trans. Signal Processing*, vol. 57, pp. 892-903, 2009.

[9] H. Guo, A. Abdi, A. Song and M. Badiey, "Delay and Doppler spreads in underwater acoustic particle velocity channels ," *J. Acoust. Soc. Am.*, vol. 129, pp. 2015-2025, 2011.

[10] C. Chen and A. Abdi, "Channel models for underwater vector transducer communication systems," in *Proc. Oceans*, Hampton Roads, VA, 2012.

[11] A. Song, A. Abdi, M. Badiey, and P. Hursky, "Experimental demonstration of underwater acoustic communication by vector sensors," *IEEE J. Oceanic Eng.*, vol. 36, pp. 454-461, 2011.

[12] H. Guo, C. Chen, A.Abdi, A. Song, M. Badiey and P. Huskey, "Capacity and statistics of measured underwater acoustic particle velocity channels," in *Proc. Meetings on Acoustics*, vol. 14, pp. 1-17, 2012.

[13] H. Guo and A. Abdi, "On the capacity of underwater acoustic particle velocity communications channels," in *Proc. Oceans*, Hampton Roads, VA, 2012.

[14] H. Cox, "Spatial correlation in arbitrary noise fields with application to ambient sea noise," *J. Acoust. Soc. Am.*, vol. 54, pp. 1289–1301, 1973.

[15] A. Abdi, J. A. Barger, and M. Kaveh, "A parametric model for the distribution of the angle of arrival and the associated correlation function and power spectrum at the mobile station," *IEEE Trans. Vehic. Technol.*, vol. 51, pp. 425-434, 2002.